Article

Worms under Pressure: Bulk Mechanical Properties of *C. elegans* Are Independent of the Cuticle

William Gilpin,[1] Sravanti Uppaluri,[2] and Clifford P. Brangwynne[2,*]
[1]Department of Physics and [2]Department of Chemical and Biological Engineering, Princeton University, Princeton, New Jersey

ABSTRACT The mechanical properties of cells and tissues play a well-known role in physiology and disease. The model organism *Caenorhabditis elegans* exhibits mechanical properties that are still poorly understood, but are thought to be dominated by its collagen-rich outer cuticle. We use a microfluidic technique to reveal that the worm responds linearly to low applied hydrostatic stress, exhibiting a volumetric compression with a bulk modulus, $\kappa = 140 \pm 20$ kPa; applying negative pressures leads to volumetric expansion of the worm, with a similar bulk modulus. Surprisingly, however, we find that a variety of collagen mutants and pharmacological perturbations targeting the cuticle do not impact the bulk modulus. Moreover, the worm exhibits dramatic stiffening at higher stresses—behavior that is also independent of the cuticle. The stress-strain curves for all conditions can be scaled onto a master equation, suggesting that *C. elegans* exhibits a universal elastic response dominated by the mechanics of pressurized internal organs.

INTRODUCTION

Cells and tissues are continually subject to a variety of mechanical loads, including gravity, hydrostatic pressure, and shear stresses, which can play a decisive role in an organism's ability to adapt and survive. The stresses and strains associated with mechanical loads have been shown to influence organisms at various length scales—from molecular-level changes such as ion channel activity (1,2) and gene expression (3), to cell differentiation (4) and tissue and organ patterning (5,6). Thus, key aspects of biological function are closely linked to the mechanics of living materials, while dysregulations of cell and tissue mechanics are associated with an array of pathologies, from skin blistering to heart disease and cancer (7,8).

A range of techniques have been developed to measure mechanics on different length scales, from the molecular scale (~1 nm) to the tissue/organ level (~1 cm to 1 m) including atomic force microscopy (9), microrheology (10), direct imaging (11), and more conventional tensile tests (12). Despite the success of these methods at the smallest and largest length scales, there are few techniques to probe the mechanics at intermediate length scales between cells and macroscopic tissues. One such intermediate system is the multicellular round worm *Caenorhabditis elegans*, a widely studied model organism. The importance of *C. elegans* mechanics is highlighted by previous studies suggesting that the worm's locomotory patterns and foraging behaviors are strongly dependent on mechanical and osmotic stresses (13–15). Indeed, external mechanical forces lead to the activation of known mechanosensory signal transduction pathways (16,17). Moreover, *C. elegans* is known to occupy diverse habitats—ranging from decaying compost to freshwater lake beds—in which it encounters a wide variety of mechanical loads (18). Combined with its genetic tractability, *C. elegans* thus represents an ideal system in which to explore the interplay of environmental loading and mechanical response at intermediate biological length scales.

The mechanics of *C. elegans* are thought to be dominated by the properties of the cuticle, a collagen-rich shell that constrains and protects the worm's body. Local stiffness measurements of the *C. elegans* cuticle have been performed using a piezoelectric transducer, which indicate that the cuticle exhibits a high elastic modulus in the range of 380 MPa (19). A similar local stiffness study using the buckling of nanowires attached to an atomic force microscope reported an elastic modulus of 457 MPa on the lateral alae, and 257 MPa in the region immediately around the lateral alae (20). These reported cuticle stiffness values are relatively large for biological tissues, comparable to hard rubber—consistent with a central role for the cuticle as the worm's exoskeleton, likely governing the mechanical response of the worm (20).

Beneath the cuticle sits the pseudocoelom, an internal cavity that surrounds the worm's digestive tract and supports its organs. Local measurements of the internal pressure in the pseudocoelom of *Ascaris*, a large, parasitic relative of *C. elegans*, have been performed using a microscale manometer inserted directly into the body cavity. These measurements suggest an internal pressure in the range of 50–100 kPa (21,22). Internal pressure is thought to induce prestrain in taut, helical collagen fiber bundles, causing a

Submitted September 8, 2014, and accepted for publication March 9, 2015.

*Correspondence: cbrangwy@princeton.edu

William Gilpin's present address is Department of Applied Physics, Stanford University, Stanford, CA.

Editor: Margaret Gardel.

© 2015 by the Biophysical Society

0006-3495/15/04/1887/12 $2.00

http://dx.doi.org/10.1016/j.bpj.2015.03.020

decrease in strain energy under bending that induces the curved appearance of many adult nematodes (23,24). Experiments on these collagen fibers in larger organisms such as fish and sharks suggest that they become stiffer under extension, and may couple to interfiber matrices throughout the organism's body in order to increase the range of body shapes that are elastically stable (24,25).

Despite the high stiffness measurements reported for the worm cuticle, an analysis based on the bending moments observed in the worm's undulatory swimming gait leads to a significantly lower estimate for the Young's modulus for the entire worm, 3.77 kPa (14); the mechanical loading in this experiment was provided by the worm's own muscles as it swims, complicating interpretation and possibly underlying the low modulus value. Another recent study measured the worm's bending modulus using deflection of the entire body under actuation from a single point (26). Calculating the Young's modulus of the worm's body yields a value ranging from 110 kPa to 1.3 MPa, depending on whether the worm is modeled as a uniform cylinder or cylindrical shell (26). The large range of reported values highlights our poor understanding of the mechanical properties of *C. elegans*. There is a clear need for elucidating the role of the cuticle, as well as the interplay of internal and external pressure, in the mechanics of the whole worm.

We demonstrate the use of a microfluidic approach to study the mechanical response of *C. elegans*. By exerting an isotropic hydrostatic pressure on young adult worms, and simultaneously monitoring their bulk mechanical response, we can calculate the compressive stress-strain curve for individual worms. We find that worms exhibit a rich mechanical response comprising an initial linear regime followed by nonlinear strain stiffening. This behavior is qualitatively similar to the results of many well-known experiments in biomechanics (12)—ranging from the mechanical response of a shark's skin (25) to the properties of cardiac muscle (27) and purified actomyosin networks (28). However, it is unusual to find such behavior at the whole-organism level, due to structural heterogeneities. Surprisingly, using a variety of genetic and pharmacological perturbations, we show that the mechanical properties are independent of the worm's cuticle. Instead, the worm exhibits a universal mechanical response that appears to reflect the intrinsic material properties of pressurized internal cells and organs.

MATERIALS AND METHODS

C. elegans culture and synchronization

C. elegans were maintained at 20°C on NGM agar plates seeded with OP50 bacteria (29,30). Strains used were wild-type (N2), *dpy-5* (e61), *dpy-10* (e128), and TP12 (*col19::gfp*) obtained from the Caenorhabditis Genetics Center (St. Paul, MN). EJ26 *gon-2*(q362) worms were a gift from Cheng Shi (Princeton University, Princeton, NJ). Intestinal cell and nuclear size were measured by crossing RT1120 (*Pvha-6::ph::gfp*) from Barth Grant (Rutgers University, New Brunswick, NJ) and JM163 (*Pelt-2::nls::h2b-dTomato::rol-6*(*su1006*)) from Jim McGhee (at the University of Calgary, Calgary, Alberta, Canada). *C. elegans* cultures were synchronized using standard hypochlorite treatment (31).

Age-synchronized young adult worms (~72 h from plating) were utilized to prevent age-related variation in mechanical properties. To study aged worms, a culture of worms was prepared in which adults were passed to a new plate immediately after the cessation of egg-laying, in order to isolate them from their progeny and prevent expansion of the population. Worms were kept well fed to prevent conflation of aging traits with starvation, and measurements were made on Day 9 after hatching. For fixation experiments, worms were treated with 4% paraformaldehyde overnight before imaging (32).

Microfluidic device fabrication

Devices were fabricated from polydimethylsiloxane (PDMS) using standard lithography techniques (33,34). Molds were prepared by spin-coating 50 μm of SU-8 50 photoresist (Microchem, Newton, MA) onto 4-inch silicon wafers and then exposing to UV light through a chrome mask. The resist was then developed, and the resulting mold was stabilized with silane before PDMS (10:1 PDMS/crosslinker) was poured onto the mold and allowed to cure overnight in a 60°C oven. Each device was peeled off of its mold, punched with inlet and outlet ports, and then plasma-treated for bonding to a glass slide. The devices were then placed in a 60°C incubator for 1 h.

Completed devices were placed overnight in standard M9 buffer to allow the PDMS to become saturated, thus preventing the devices from absorbing water when pressure was applied during experiments (31). Before each experiment, devices were removed from the M9 and placed in a 60°C oven for 30 min to remove condensation that tends to form on the outer surface of the device, which reduces image quality.

Image acquisition

Healthy young adult worms were identified based on the observation of 6–10 eggs visible in the gonad, neatly lined up along the body axis—~72 h after hatching. Several such worms were individually picked and loaded into the imaging chamber through the inlet port. These worms were exposed to a 10% levamisole solution for ~10 min (until they were paralyzed). The outlet of the device was plugged and the device was then transferred to the microscope and syringe pump for imaging.

Bright-field images were acquired using a model No. M205FA fluorescence stereomicroscope at 34× optical zoom (Leica Microsystems, Wetzlar, Germany). A length of PTFE syringe tubing filled with additional levamisole solution was connected to the inlet of the device, and the other end of the tubing was connected to a gastight syringe (Hamilton, Reno, NV) containing 2.5 mL of air. The syringe was then placed within a programmable syringe pump (Chemyx, Stafford, TX).

For the experiment, pressure was gradually applied by setting a low flow rate on the syringe pump—because of the plug at the outlet of the device, the syringe pump gradually compressed the air in the gastight syringe, resulting in a proportional increase in hydrostatic pressure in both the air and the solution containing the worm (see below for pressure calculation). Bright-field images were taken at frequent intervals as illustrated in Fig. 1 *A*.

Fluorescence images shown in Fig. 1 *C* and later in Fig. 7 were acquired with a CSU-X1 spinning disk confocal (Yokogawa, Tokyo, Japan) on an Axio Observer Z1 (Carl Zeiss, Oberkochen, Germany) equipped with a 63× oil objective. The differential interference contrast images shown later in Fig. 6 were obtained with a model No. TE300 microscope (Nikon, Melville, NY) using a 60× oil objective.

Image analysis

Time-lapse sequences of images were processed using IMAGEJ (National Institutes of Health, Bethesda, MD) (35) and MATLAB (The MathWorks,

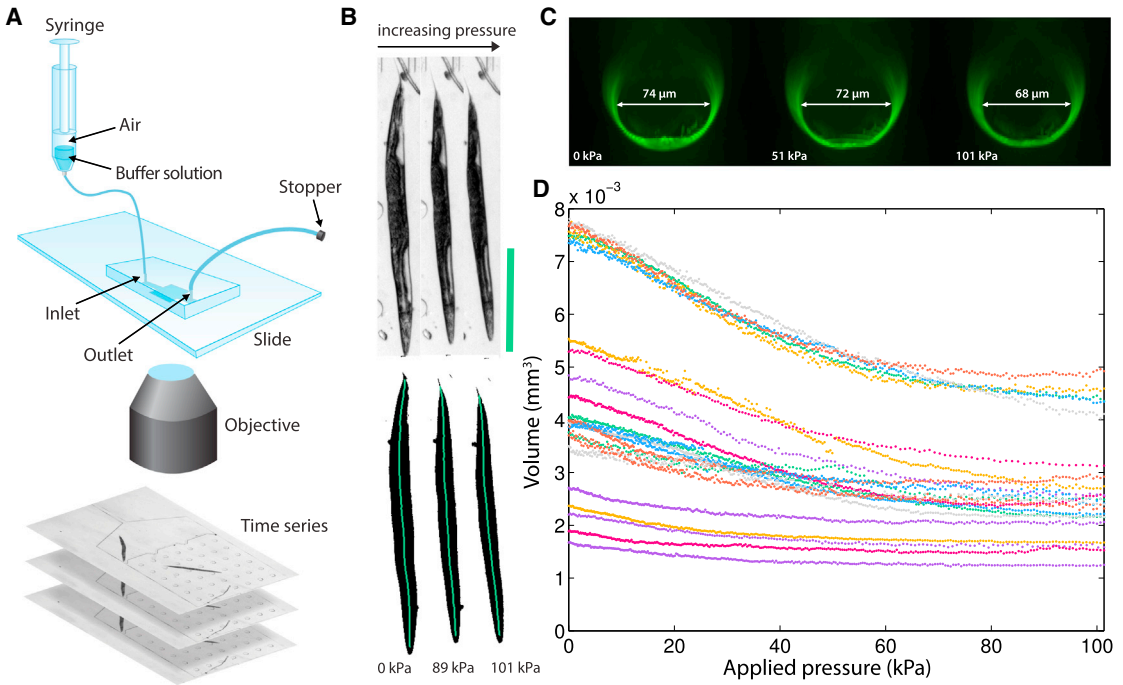

FIGURE 1 (*A*) Schematic of the experimental setup, showing the syringe, microfluidic device, microscope, and resulting time series of images. (*B*) The steps of the image processing routine for representative images of a single time series: the original images are binarized (described in Materials and Methods), and a central line is fit to the body in order to measure length. Scale bar, 500 μm. (*C*) Cross-sectional view of a worm with a fluorescent-tagged cuticle undergoing deformation. (*D*) Volume versus pressure curves for several wild-type *C. elegans* worms.

Natick, MA). Individual sequences of images were cropped and corrected for exposure using IMAGEJ, and then binarized in MATLAB. The binary images were manually inspected and closing and fill operations were made if required. The worm's projected area at each time point was obtained using the binarized image.

To determine the length of the worm, a contour-pruning skeletonization operation was applied to the binary image, which serves to generate a one-pixel-wide backbone corresponding the worm's body axis (36). The output of these image processing steps is shown in Fig. 1 *B*.

Because the worm is approximately radially symmetric, we treat the worm as a cylinder (14,19,37) and estimate changes in the body volume from its area and the length, using

$$V(p) = (\pi/4)A^2(p)/L(p).$$

Here A is the area of the worm image in the microscope viewing field, and L is the length of a principal curve corresponding to longest axis of a convex representation of the image (38). The time series of images can thus be transformed into a two-dimensional data set consisting of the volume of the worm and the pressure within the microfluidic device (Fig. 1, *B* and *D*).

For nuclear volume, the major and minor axes of the thresholded image shown later in Fig. 7 were used to approximate the nucleus to an ellipsoid. Intestinal cells were approximated to half-cylinders and length and radius were measured manually.

Determination of pressure within the microfluidic device

The Fusion 200 syringe pump (Chemyx) can decrease the volume within a syringe at a fixed rate. To map the volume in a syringe to an effective pressure within the plugged device, the air within the syringe is assumed to be approximately ideal, allowing the pressure at a given time point (and syringe volume) to be inferred using Boyle's law,

$$P(t) = P_0(V_0/V(t)),$$

where $P_0 = 101.325$ kPa (ambient pressure) and V_0 is the initial volume of air in the syringe. The pump operates by decreasing the volume in the syringe at a fixed rate, such that $V(t) = V_0 \times (1 - kt)$. Here k represents the fractional rate $k = (V_f - V_0)/V_0T$, where V_f is the final volume measured in the syringe, and T is the total time period over which the pump acts to decrease the volume from V_0 to V_f. For the experiments reported here, which used a Hamilton gastight syringe and a Fusion 200 syringe pump (Chemyx), $V_0 = 2.5$ mL, $V_f = 1.25$ mL, and $T = 15$ min. This corresponds to $k = 5.\overline{5} \times 10^{-4}$ s^{-1}. For experiments in which the rate of pressure application needs to be varied, the total pumping period T is varied.

Error in the use of Boyle's law to calculate pressure may arise over very short timescales, if the syringe is depressed very quickly, because the system does not have time to adiabatically change state and instead equilibrates after the cessation of pressurization. A probe of the timescale of this effect and a control experiment used to determine whether the final pressure in the device matched that predicted by Boyle's law (not shown) are consistent with reports that Boyle's law is generally accurate at room temperature to within a factor of 5%; the error arises primarily due to humidity and the presence of gases that strongly adsorb to surfaces (39). The pressure within the device was also directly confirmed using a mechanical gauge, and the results are shown and discussed in Fig. S1 in the Supporting Material. As discussed below, water appears to enter and exit the worm quickly enough that for all pressurization rates tested (all slower than 20 kPa/min), the transient equilibration of pressure gradients was not a limiting factor in the deformation. Additionally, we found that the worm's mechanical response did not depend on pressurization rate, and we thus arbitrarily chose to linearly increase the pressure over 15 min, to attain the maximum pressure of 1 atm (101 kPa).

RESULTS

Determination of the effective bulk modulus of young *C. elegans* adults

Young adult *C. elegans* hermaphrodites (~3 days posthatching) were loaded into the microfluidic chamber, and subsequently anesthetized with a stream of 10% levamisole. When pressure is applied using the syringe, the worm body smoothly decreases in size. This size decrease is apparent in the microscopy time series as a smooth decrease in the projected area of the worm, as shown in Fig. 1. Using a transgenic worm with *COL-19::GFP*, the cross-section of the worm can be seen to also decrease uniformly during pressure application; analysis of the average radius in each frame confirms that the final relative radial strain matches that of the worm's entire body—suggesting that the worm deforms isotropically. We can therefore monitor worm volume as a function of applied hydrostatic stress (see Materials and Methods).

The decrease in worm volume corresponds to a volumetric strain, $\epsilon = |\Delta V|/V_0$. We can thus transform the data to plot hydrostatic stress (σ) versus strain, as shown in Fig. 2. These stress-strain curves all exhibit an approximately linear regime at small stress/strain, followed by a nonlinear strain stiffening regime, during which there is little additional compression even at large applied pressures. The initial slope of the stress-strain curve (linear regime) provides a measure of the bulk modulus of each worm's body,

$$\kappa = \frac{\Delta\sigma}{\Delta\epsilon} = V_0\frac{\Delta P}{|\Delta V|}.$$

We find no dependence of the bulk modulus on the initial worm size, over nearly an order of magnitude in volume (Fig. 2 *B*); this suggests that the calculation of the volume correctly addresses the geometry of the deformation in this linear regime, and that this measurement reflects a true bulk modulus. For these anesthetized young adult worms, we obtain an average bulk modulus of $\kappa = 140 \pm 20$ kPa ($N = 22$).

The worm responds immediately to the application of increased hydrostatic pressure, suggesting this response reflects passive mechanical properties of the worm, rather than some active biological pressure response. To test this, several worms were killed using the toxin sodium azide. These dead worms were found to exhibit no significant difference in modulus compared with living worms in the linear regime, as indicated by the similar form of the curves in Fig. S2. Thus, the observed stiffness is a purely passive mechanical property of *C. elegans*, consistent with previous studies (26).

Worms expand under negative applied pressure

By inverting the direction of the syringe pump and successively increasing the volume in the syringe, a negative pressure was applied to several worms. Interestingly, the worms exhibit a corresponding expansion under negative applied pressure, as shown in the inset of Fig. 3; the resulting stress-strain curves are shown in the main figure. Overall, the expanded worms exhibited a modulus $\kappa = 130 \pm 20$ kPa ($N = 4$), not significantly different from that of the compressed worms. Thus, there is no extension-compression asymmetry within the system, suggesting that the observed modulus does not result from a specific rearrangement of internal structures, but instead arises from their combined mechanical properties and internal couplings.

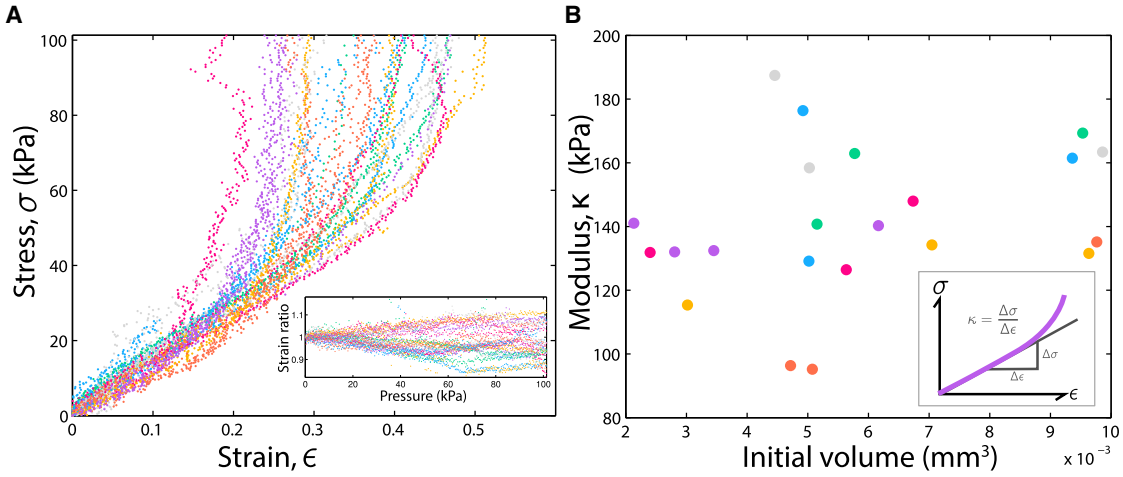

FIGURE 2 The result of applying a linearly increasing pressure to young adult *C elegans*. Individual colors correspond to individual experiments with a single worm; colors assigned to specific individuals are consistent across plots. (*A*) Hydrostatic stress versus calculated volumetric strain for individual worms. (*Inset*) Ratio of radial and longitudinal strains shows effective modulus is the same along both directions. (*B*) The bulk moduli resulting from fitting lines to the initial portions of the curves in (*A*), plotted against the volume of the worm before the initiation of pressurization. All modulus fitting errors due to data scatter are smaller than the thickness of the plot markers.

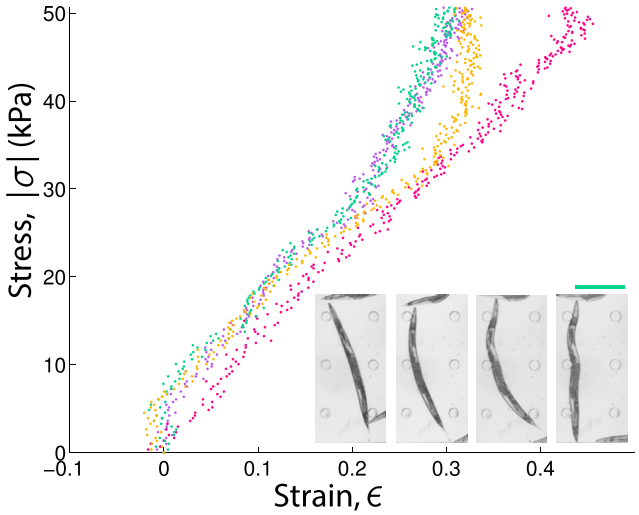

FIGURE 3 Stress-strain curves when negative pressure is applied to the worm, causing expansion rather than contraction. (*Inset*) Representative body shapes. Scale bar, 500 μm. To see this figure in color, go online.

For the remainder of this work, we choose to focus on compression experiments because of their greater working range (101 kPa by halving the gas volume in the pump, instead of 51 kPa by doubling the gas volume), as well as improvements in image quality due to greater regularity in the shapes of the compressed worms. Compression experiments also provide additional information about the nonlinear response of the worm under large applied stresses, an effect not observed when negative pressure is applied.

The mechanical response exhibits no hysteresis and is independent of stress application rate

To further characterize the origins of the observed deformation, a pressure sequence was applied corresponding to one-and-a-half periods of a sawtooth waveform: as in previous experiments, pressure was first steadily increased to a maximum value of 101.325 kPa; but it was then reduced back to atmospheric pressure at the same rate, and then increased once again. The resulting volumetric changes in the worm are shown in Fig. 4 *A* for three different pressurization rates with the corresponding stress-strain curves. The resulting stress-strain plot displays no clear hysteresis, as evidenced by the negligible area between the curves corresponding to compression and decompression. This indicates that viscous relaxation does not strongly affect the whole-body mechanics over the three timescales probed, and it also confirms that repeated cycles of prestressing are not necessary to induce a steady-state mechanical response (27). Moreover, during pressure release and subsequent repressurization, the worm body shape recovers. These findings are consistent with a purely elastic mechanical response of the worm.

We next tested whether the measured mechanical response depended on the rate at which pressure is applied. Varying the pressure rate from roughly 0.1 to 0.6 kPa/s led to no significant trend in the resulting modulus (Fig. 4 *B*). The independence of the modulus from the stress rate over the experimentally accessible timescales suggests that the transport of water within the worm's body (and thus equilibration of pressure) is not a limiting factor in the deformation; this is consistent with calculations of the expected timescale for poroelastic effects, $\tau \sim 10^{-2}$ s, suggesting that any hydrodynamic draining occurs very quickly (see the Supporting Material) (40,41).

The modulus is determined by internal structures and not the cuticle

Previous studies have concluded that the collagen-rich cuticle plays an important role in determining the local stiffness (19,20) and bending rigidity (26) of worms. To test the role of the cuticle, worms were exposed to proteinase K, an enzyme that degrades cuticle proteins (22,42). The same pressurization experiment was then performed on the treated worms, resulting in the traces shown in Fig. 5 *A*. Surprisingly, the modulus of proteinase K-treated worms, $\kappa = 130 \pm 50$ kPa, was not statistically different from that of untreated worms.

While *C. elegans* grow to sexually mature adults within 2–3 days, the average lifespan extends significantly beyond this, to roughly 10 days (43). These late-stage adult worms are known to exhibit aging, which includes significant changes in cuticle morphology (44) and may involve collagen degradation (45). In our experiments, we noted several differences from younger adults, including a wrinkled, irregular appearance, reduced locomotion, and a cramped, heterogenous internal structure due to unlaid eggs. Surprisingly, however, when the worms were exposed to the same pressurization treatment (Fig. 5 *B*), they exhibited almost the same response as young adult worms. The modulus was lower than that measured for younger adult worms, $K = 115 \pm 20$ kPa, but this effect was not statistically significant. This suggests that changes to the cuticle and other structures during aging do not significantly affect the bulk material properties of the worm.

Because aging gives rise to pleiotropic effects other than degradation of cuticle integrity, we sought more specific perturbations of the cuticle. The dumpy (Dpy) phenotype is caused by one of several mutations to proteins key to cuticle structure, including collagens (46,47). For example, *dpy-10* worms have a mutation in a collagen gene important in morphogenesis and development, while *dpy-5* worms have a mutated cuticle procollagen gene. These and other Dpy worms exhibit a smaller aspect ratio, growing to approximately half the typical adult size, but with double the width (Fig. 5, *C* and *D*, *inset*). Previous studies probing

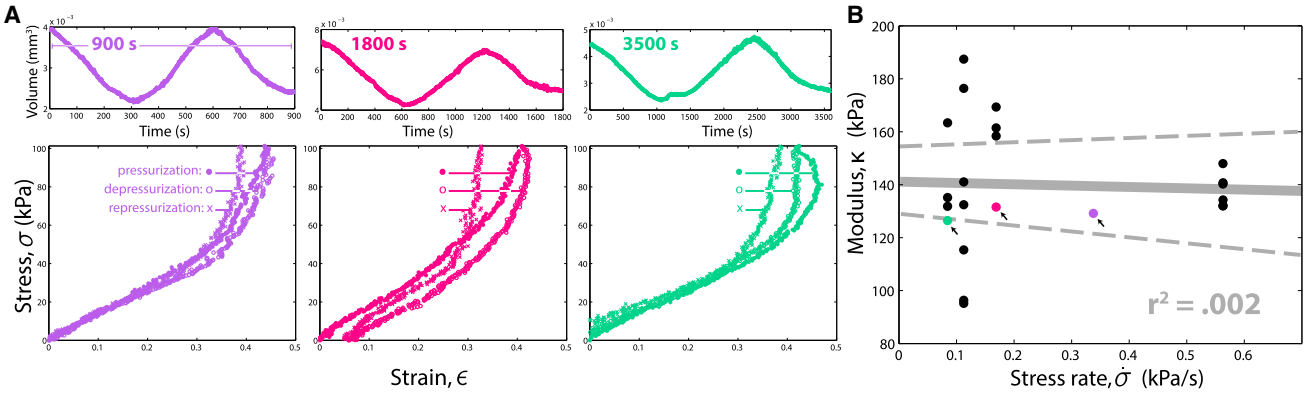

FIGURE 4 (*A*) The result of applying pressure to the bodies of anesthetized worms over three different timescales; the upper portion of each plot represents a time series of the volume of the worm's body as the pressure sequence was applied, and the lower portions represent the same data transformed into a stress-strain curve. In the stress-strain curves, different markers have been used to differentiate the pressurization, depressurization, and repressurization processes. (*B*) The modulus as a function of rate for different young adult worms, with the cases in (*A*) colored. (*Arrows*) Trials in (*A*) indicated. (*Shaded line*) Linear fit to the data; the 95% confidence interval for the fit (*dashed lines*) includes the case of zero slope, and the correlation coefficient (*inset*) is much less than 1, indicating no significant correlation between the modulus and the rate of pressure application over the range studied. All modulus fitting errors due to data scatter are smaller than the thickness of the plot markers. To see this figure in color, go online.

the local material properties of the worm have confirmed that Dpy worms exhibit an ~25% softer cuticle (19), consistent with a significant disruption of cuticle structure. However, we found that both *dpy-5* and *dpy-10* worms exhibited no significant difference in their bulk modulus compared with wild-type worms (Fig. 5, $K = 120 \pm 40$ kPa and $K = 120 \pm 30$ kPa, respectively). This suggests that changes in cuticle structure and mechanics in worms do not play a significant role in the bulk modulus of the worm. Moreover, the strain at which worms exhibit an asymptotic stiffening was not measurably different for Dpy and wild-type, suggesting that this nonlinear stiffening regime is also not a consequence of the cuticle, but instead due to structures within the worm.

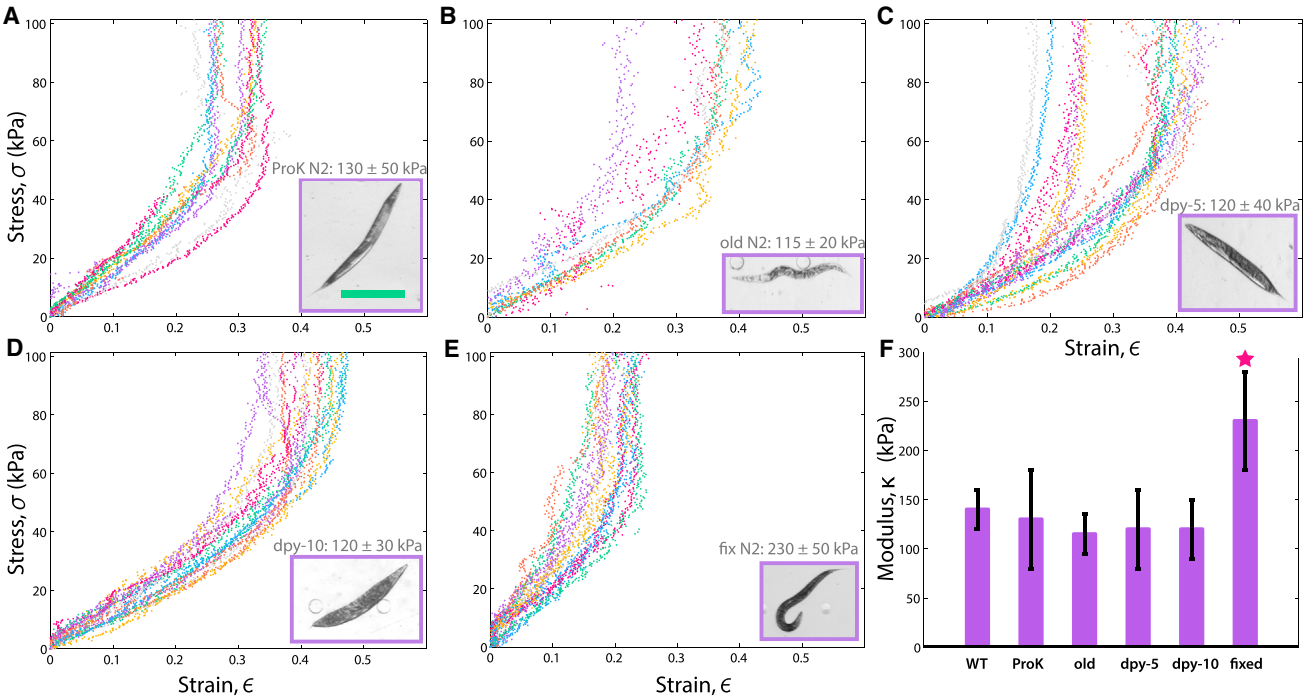

FIGURE 5 (*A*) Stress-strain curves for wild-type young adult *C. elegans* treated with the enzyme proteinase K. Scale bar, 500 μm; all images in all figures are at the same scale. (*B*) Stress-strain curves for nine-day-old wild-type worms; (*C*) for *dpy-5* mutants; (*D*) for *dpy-10* mutants; and (*E*) for wild-type PFA-fixed worms. (*F*) A bar chart indicating the measured moduli for each of the treatments (standard deviation overlaid); fixed worms represent the only condition with a statistically significant difference from wild-type (unpaired *t*-test, $N_1 = 22$, $N_2 = 12$, $p < 0.001$). To see this figure in color, go online.

Because the cuticle does not appear to play a role, we sought to test the role of the internal organs and pseudocoelom of the worm (22). Adult worms were treated with the fixation agent paraformaldehyde (PFA), which induces cross-linking in tissues (31). When fixed worms are placed in the microfluidic device and pressurized, they exhibit a markedly higher modulus, $K = 230 \pm 50$ kPa, which is nearly twofold larger than all other treatments and significantly greater than the wild-type (Fig. 5 *E*). Because the cuticle comprises a negligible fraction of the total volume of the worm on which the PFA acts, this high modulus suggests that the bulk material properties of the worm arise primarily from its internal structures.

Structural deformation of internal organs

To elucidate the microscopic effects of applied pressure on the internal structure of the worm, we performed high-magnification differential-interference contrast imaging of portions of the worm during compression. Subsequent analysis of these microscopic images using digital image correlation methods (see the Supporting Material) allowed for determination of the time-varying displacement field of the worm's internal structures as they deform under applied stress (*middle panels* of Fig. 6 *A*) (48). The strain can then be calculated using the Cauchy transformation between displacement and strain in a body undergoing pure deformation (49),

$$\epsilon_{ij} = \frac{1}{2}\left(\frac{\partial u_i}{\partial x_j} + \frac{\partial u_j}{\partial x_i}\right),$$

where $\mathbf{u}(\mathbf{x})$ are the calculated displacements for all points $\mathbf{x}$ in a pair of consecutive images, and both indices run over 1 and 2 for the two-dimensional microscopy images. In order to generate a single field representing the dominant strain observed at each location in the displacement field at each timepoint, the 2×2 strain matrix ϵ was diagonalized, and the eigenvalue with the maximum magnitude was used as an estimate of the maximum strain occurring along the principal eigenvector. A representative set of images, corresponding to the calculated displacement field and strain map, are shown in the lower panels of Fig. 6 *A*.

As indicated in Fig. 6, while the entire worm undergoes deformation, the gonad and maturing oocytes appear to move relative to the cuticle during all phases of the deformation. The individual oocytes undergo considerable deformation, as indicated by their crescent shape (outlined in the *top-right panel* of Fig. 6 *A*). The motion of the oocytes relative to the cuticle during isotropic loading suggests that the two structures have distinct mechanical properties. The strain maps in the figure also illustrate a high relative degree of strain within the gonad at higher stress, which implies that the gonad deforms more than other internal worm structures—suggesting that it could play an important role in the measured compressive modulus.

To test the hypothesis that the gonad plays an important role in the bulk mechanical properties of the worm, we utilized worms bearing a gon-2 mutation, in which larvae can grow to adulthood without ever developing a gonad (50). The sterile worms were found to exhibit a behavior similar to wild-type worms, with a linear regime at small stress/strain, and a nonlinear stiffening regime at higher stress/strain. Importantly, however, in the absence of a gonad the worms were significantly softer, with a bulk modulus of 100 ± 14 kPa (Fig. 6 *B*). Thus the gonad (and likely other internal organs) plays an important role in determining the mechanical properties of the worm.

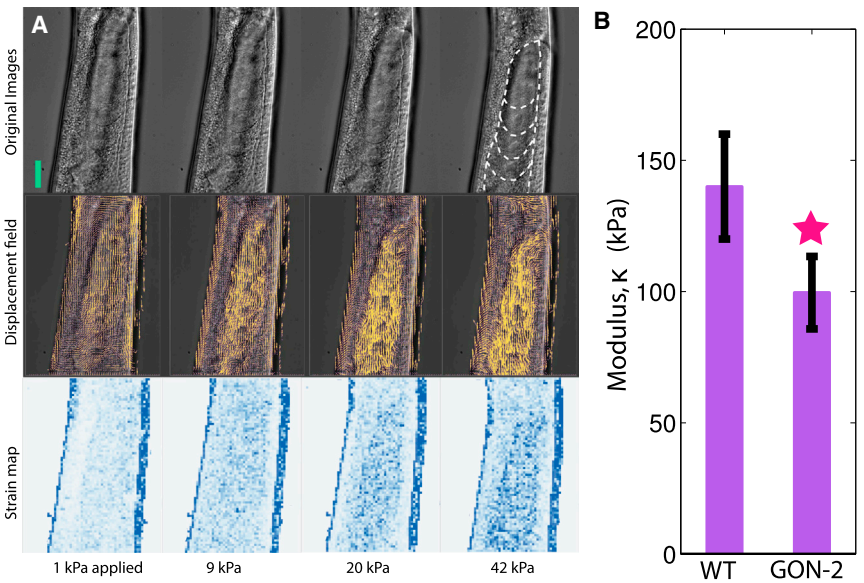

FIGURE 6 (*A*) Time series of the effects of pressure on internal structures of the worm. (*Top*) Four representative, sequential images of the gonad and oocytes as pressure is applied. In the last panel, individual oocytes comprising the gonad have been outlined (*dashed line*). (*Middle*) The displacement fields corresponding to each time point, calculated from the entire time series and overlaid on the chosen images. (*Bottom*) Magnitude of the principal strain associated with the displacement fields. Darker color indicates higher relative strain. The apparently high strain near the border of the worm is an artifact of the cross-correlation calculation. Scale bar, 25 μm. (*B*) Bulk modulus of gonadless worms (GON-2) is significantly lower than wild-type (unpaired *t*-test, $N_1 = 22$, $N_2 = 9$, $p < 0.001$). The standard deviation is overlaid.

Structural deformation of cells and organelles

To further elucidate the microscopic origins of the measured elastic response, high-magnification experiments were performed on worms with intestinal cell membranes tagged with green fluorescence protein (GFP) and their nuclei tagged with dTomato. The shape and arrangement of the cells before and after the application of pressure is shown in Fig. 7 *A*. As with the whole worm, cells underwent approximately isotropic deformation, with all tagged structures imaged exhibiting compression as a result of the applied pressure. These observations provide additional evidence that compression of internal organs, including the gonad and intestine, rather than just the cuticle, plays a role in the observed mechanical response of the organism.

When the final and initial volume of individual intestinal cells and nuclei are compared (Fig. 7 *B*), it is clear that the relative deformation for both types of structures is very similar—they deform together. Strikingly, when the initial and final volumes for the entire worms shown in Fig. 2 are added to the curve, the resulting points obey the same trend, despite corresponding to volumes two orders-of-magnitude larger than the cells.

The slope of each cluster of points on the graph corresponds to the maximal strain, or the location of the vertical asymptote in stress-strain curves like those shown in Fig. 2. That structures at three very different length scales exhibit an identical maximum strain suggests that mechanical coupling among multiple internal structures underlies the mechanical response of the worm.

The worm undergoes nonlinear stiffening at high applied stress

At higher pressures, the elastic response of individual worms under all of the conditions tested began to diverge, such that even at high compressive stress the worms underwent little additional deformation. Thus, worms exhibit increasing effective stiffness with increasing applied stress, a phenomenon widely observed in soft matter, including other living materials (27,28,51).

This stiffening behavior reflects an apparent asymptote at a maximum strain, ϵ_0. The simplest functional form that fits this behavior is a logarithmic function,

$$\sigma = -\sigma_0 \ln(1 - \epsilon/\epsilon_0). \quad (1)$$

Here the parameter, σ_0, represents a characteristic stress at the onset of nonlinearity. The curves from each individual worm can be scaled together by fitting each stress-strain data set to this logarithmic function, and then nondimensionalizing the fitted data by dividing each point by parameters (ϵ_0, σ_0) resulting from the best fit to that data set. The resulting plot of the scaled data, σ/σ_0 versus ϵ/ϵ_0 for every treatment, is shown in Fig. 8 *A*.

Defining the elastic modulus as the derivative, $K \equiv \partial\sigma/\partial\epsilon$, from the logarithmic function we obtain an expression $K = \kappa_0/(1 - \epsilon/\epsilon_0)$, where $\kappa_0 = \sigma_0/\epsilon_0$ is the coefficient of the first-order term in a Taylor expansion of $\sigma(\epsilon)$, corresponding to low-strain modulus in the linear regime. As a consistency check, a plot of σ_0 versus ϵ_0 (*inset* in Fig. 8 *A*) exhibits a slope near that given independently by fitting the linear portion to a line, $\kappa = 140$ kPa. Moreover, the two data sets for which the worm displayed a significantly different modulus than wild-type, the fixed worms and the GON-2 mutants, appear to have higher and lower slopes, respectively, than the rest of the data (*enclosing ovals*, Fig. 8 *A*, *inset*)—although this was less significant for the GON-2 data.

DISCUSSION

Functional significance of *C. elegans* mechanics

As with every organism, *C. elegans* is subject to pressure and numerous other mechanical loads that can strongly impact biological function. Mechanical forces are known to play a direct role in triggering signal transduction pathways in *C. elegans* (16,17). Because the adult worm has only 22 specialized nerve cells for mechanotransduction, the bulk mechanical properties of the organism will determine how mechanical stimuli are distributed across these

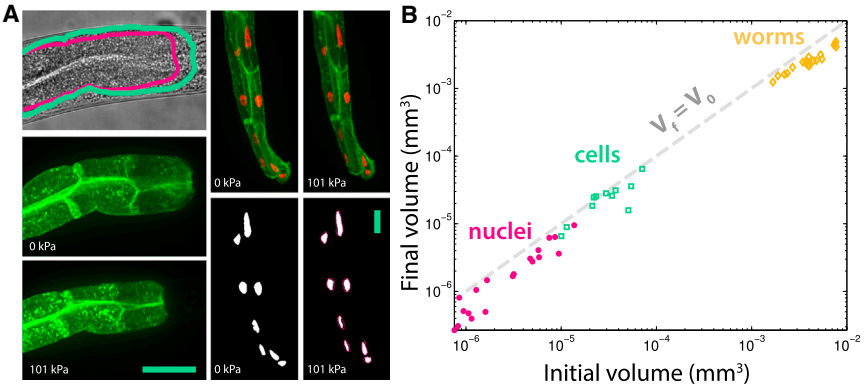

FIGURE 7 (*A*) (*Left*) The outline of the intestine before (*green*) and after (*magenta*) the application of 101 kPa of pressure, overlaid on a bright-field image; cell membrane-tagged images from the same sample show uniform compression of internal structures. (*Right*) Two-channel fluorescence images showing compression of green-tagged cells and red-tagged nuclei before and after 101 kPa are applied. Binarized outlines of cells are shown below each image. Scale bars, 50 μm. (*B*) The final volume versus the initial volume computed from fluorescence images of cells and nuclei (five worms), as well as the final and initial volumes computed for the worms shown in Fig. 2. (*Dashed line*) Zero strain case in which the final volume equals the initial volume.

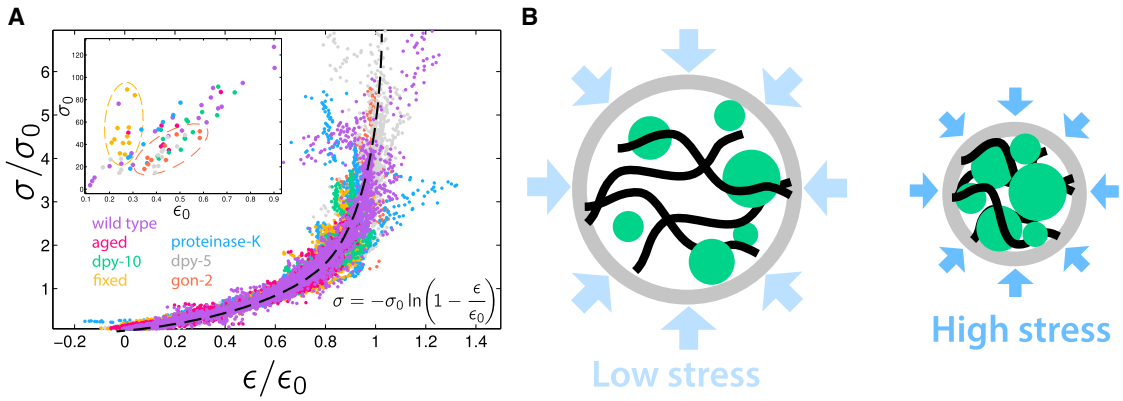

FIGURE 8 (*A*) The stress-strain curves for all data, normalized by the parameters of a best-fit logarithmic curve (equation shown on plot; *dashed overlay*). (*Inset*) A plot of the best-fit parameters shows a linear correlation with a slope near 140 kPa. The fixed data have a higher slope on the plot (*yellow oval*); additionally, the GON-2 data (*orange oval*) also appear separated from the other data points, although this effect is not significant. (*B*) A schematic showing a possible mechanism for the observed stiffening behavior, in which a network sustains elasticity at low stress, but nondeformable components jam together at high stress.

specialized cells—mechanical coupling thus allows short timescale coupling of different mechanosensory neurons (52). More directly, the stiffness of the body affects how sensitive these neurons will be to stimuli of various magnitudes. This suggests that the bulk mechanical properties are essential for understanding the feedback between the nervous system and mechanics during rapid processes, such as locomotion (14).

At ecological scales, the unique mechanical response of the worm may be related to its adaptation to the soil environment it is known to inhabit (18). A bulk modulus ~1 atm would lead to observable strains (~10% if the worm moves downwards a distance of 1 m in the water column), suggesting that a soft, hydraulically reinforced body plan may allow the worm to inhabit a greater range of environments. Similarly, a soft, isotropically deformable body may allow the worm to optimize its swimming mechanism for heterogenous or pressurized environments, as there is known mechanical feedback between the worm's environment and its ability to swim (13,53).

Using hydrostatic pressure to probe *C. elegans* mechanics

The method we describe here utilizes the application of hydrostatic pressure to measure the whole-body material properties of *C. elegans* worms. The method may be integrated within more complicated microfluidic platforms, and could thus be suitable for high-throughput studies. However, despite the potential power of this technique, there are fundamental and intriguing questions that remain about the biophysical origin of the observed volumetric changes in response to applied hydrostatic pressure. Order-of-magnitude calculations based on estimated pore sizes suggest that if the worm were a simple cylindrical biopolymeric hydrogel, hydrostatic pressure would equilibrate over the relatively slow timescales of the experiment (see the Supporting Material); this corresponds to the so-called drained limit in the literature on poroelasticity, and is consistent with the rate-independence of the data (Fig. 4) (40,41). But, if the pressure inside the worm were to equal that on the outside, why should the worm deform at all?

A hint to understanding this paradox comes from previous studies, which have suggested that worms maintain an elevated internal pressure (21) that may be important for maintaining their cylindrical shape. Consistent with these reports, we find that when mechanically punctured using a fine microneedle, *C. elegans* rapidly expel their internal organs, like a pressurized balloon, as shown in the inset of Fig. 9. Given the intrinsically elevated internal pressure, the simplest model is one in which the internal pressure is maintained at a constant value even under changes in the external pressure (Fig. 9); this could be an important adaptation mechanism for maintaining shape in different soil or aqueous depths, corresponding to changed external pressures. In one dimension, an internally pressurized worm would be governed by the relation

$$(P_{\text{in}} - P_{\text{out}}) = K\Delta x, \tag{2}$$

where Δx is the degree of contraction of the body (e.g., along the radial direction). K is an apparent spring constant; P_{in} is the internal pressure, estimated to be in the range of 150–200 kPa (21); and P_{out} is the externally applied pressure plus the ambient atmospheric pressure, $P_{\text{out}} = P_{\text{applied}} + P_{\text{atmospheric}} = P_{\text{applied}} + 101.325$ kPa. Physically, as the applied pressure increases, water moves out of the worm to keep the internal pressure constant. The applied force is thus balanced by the elastic deformation of the body. A simple diagram of this model is shown in Fig. 9 *B*.

This simple model provides a mechanism for the symmetric, reversible deformation of the worm under compressive

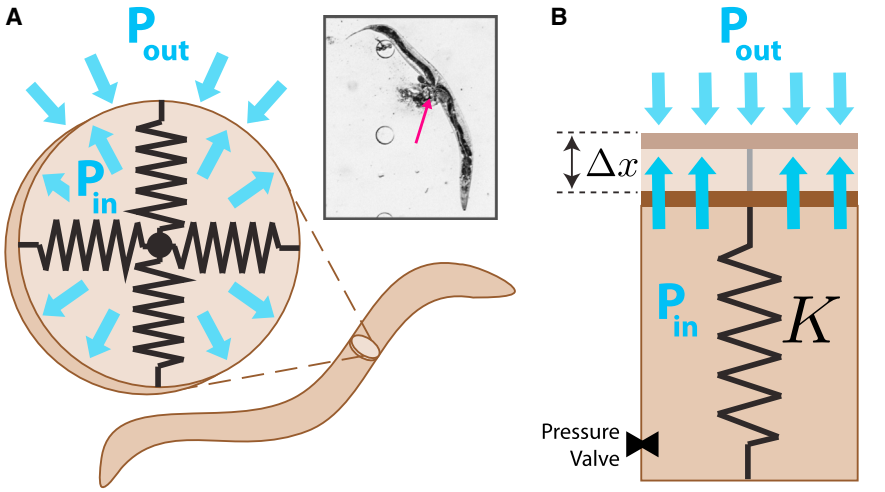

FIGURE 9 (*A*) The worm can be thought of as a stack of radially symmetric springs stretched to compensate for different internal and external pressures. (*Inset*) After the worm is punctured with a fine needle, internal organs are rapidly expelled, indicating high internal pressure (puncture location indicated by *magenta arrow*). (*B*) The system can be reduced to a one-dimensional model containing a valve that regulates the internal pressure. To see this figure in color, go online.

and extensive loading, and it illustrates the manner by which experiments conducted at many different time- and length scales are able to reveal a single linear bulk modulus for the worm ($\kappa \propto K$). The nonlinear response of the worm observed at large compressive forces likely represents the breakdown of this equation when crowding effects within the worm become important. Intriguingly, an article by Yin and Kuebler (2) predicts that, in the absence of external pressure from a syringe pump, the worm's body has a characteristic extension due to its higher internal pressure. This suggests that, when the applied pressure exceeds the difference between the resting internal pressure and atmospheric pressure, this prestrain vanishes and the worm's body enters a stage corresponding to zero net elastic deformation ($\Delta x = 0$).

Origin of nonlinear response

The universal form of these stress-strain curves, approximated by a logarithmic function with a well-defined asymptote, suggests that a robust physical mechanism underlies this behavior. One possibility is that this arises from the known nonlinear response of helical collagen fibers to large applied stresses (24). However, this effect alone cannot explain the isotropy of the deformation along the long and short axes of the worm's body (Fig. 2) or the observed compression of structures over many different length scales (Fig. 7). Another possible contributing factor is that the helical filaments are strongly mechanically coordinated with other structures and interfiber matrices within the worm—an effect that has been observed in the collagen fibers of other nematodes as well as in more complex organisms (24,25).

The abruptness of the strain asymptote ϵ_0 in Fig. 8 is unusual for the collective response of coupled nonlinear elastic elements; previous studies that have reported a non-Hookean, J-shaped stress-strain relation in bulk tissues (e.g., cardiac muscle or tendons) have identified a power-law dependence and hardening over orders-of-magnitude of stress increase, rather than over the relatively small pressure range used in our experiments (12,54). One hypothesis for the origin of such a well-defined upper-limit on strain is that internal structures undergo jamming and the effective stiffness of the worm diverges. Similar behavior is widely observed in the jamming of emulsions or other soft colloidal suspensions, and the rearrangement of the gonad relative to other organs in Fig. 6 suggests that the internal volume may eventually become small enough that the organs, cells, and subcellular structures crowd together and cease to rearrange, leading to divergence in the apparent modulus (55–57). The linear and nonlinear mechanical properties of the worm would thus arise from two key parameters: 1) the effective volume fraction occupied by relatively incompressible internal structures, ϕ; and 2) the intrinsic modulus of these internal structures, κ_0. A schematic is shown in Fig. 8 *B*, in which low stresses cause rearrangement and network compression, but high stresses cause jamming and stiffening. The existence of a well-defined upper-limit on strain, ϵ_0, which is conserved across length scales ranging from the entire worm to individual nuclei (Fig. 7), underscores how a jamming-like physical limit on volume compression could determine the response of the worm to high stresses.

Cuticle-independent mechanical response

A key finding of this study is that both the linear elastic modulus and the nonlinear stiffening do not depend strongly on the worm's collagen-rich cuticle. This suggests that traditional models describing the compression of helical collagen fiber bundles in cylindrical animals (24,54) may have limited applicability for understanding the whole-body mechanics of *C. elegans*. Importantly, this does not imply that the cuticle is a mechanically soft material. The cuticle is known to be comprised of a dense collagenous

shell, and previous work using local mechanical deformation experiments has suggested that it has a very high stiffness on the order of 257–457 MPa (19,20). However, it is known to be very thin (0.5 μm, roughly 2% of the diameter of the worm), and thus its contribution to the overall stiffness of the worm need not be significant (42). Consistent with this, our measured value for the worm bulk modulus, $\kappa = 140 \pm 20$ kPa, is in close agreement with bending measurements of the worm body (26), provided the worm is modeled as a uniform cylinder, rather than as a hollow tube comprised solely of the cuticle. The worm's bulk mechanical properties thus reflect coarse-grained properties of the entire worm, rather than its cuticle alone.

A number of studies have demonstrated that mutations affecting collagen proteins result in strong morphological phenotypes, including the severely misshapen Dpy worms analyzed in our study (47). Together with the findings we report here, this suggests that the cuticle exhibits a remarkable set of material properties, at once functioning as a thin scaffold that sculpts the morphology of the developing worm, while at the same time being remarkably flexible and deformable. Further study will be necessary to elucidate these multifunctional material properties, and their connection to the growth and form of the developing worm.

SUPPORTING MATERIAL

Supporting Material and two figures are available at http://www.biophysj.org/biophysj/supplemental/S0006-3495(15)00281-7.

ACKNOWLEDGMENTS

We thank Stephanie Weber, Marina Feric, Josh Shaevitz, Tommy Angelini, Chase Broedersz, and Margaret Gardel for helpful discussions.

W.G. was supported in part by The Fred Fox Fellowship, The Princeton Class of 1984 Memorial Fund, The Princeton Class of 1955 Senior Thesis Fund, and the Princeton Class of 1930 Fellowship. Some strains were provided by the Caenorhabditis Genetics Center, which is funded by the National Institutes of Health Office of Research Infrastructure Programs (No. P40 OD010440). This work was also supported by the National Institutes of Health Director's New Innovator Award (No. 1DP2GM105437-01), the Searle Scholars Program, and a National Science Foundation CAREER Award (No. 1253035).

REFERENCES

1. Coste, B., B. Xiao, …, A. Patapoutian. 2012. Piezo proteins are pore-forming subunits of mechanically activated channels. *Nature.* 483:176–181.
2. Yin, J., and W. M. Kuebler. 2010. Mechanotransduction by TRP channels: general concepts and specific role in the vasculature. *Cell Biochem. Biophys*. 56:1–18.
3. Lehoux, S., and A. Tedgui. 2003. Cellular mechanics and gene expression in blood vessels. *J. Biomech*. 36:631–643.
4. Engler, A. J., S. Sen, …, D. E. Discher. 2006. Matrix elasticity directs stem cell lineage specification. *Cell.* 126:677–689.
5. Prendergast, P. J., R. Huiskes, and K. Søballe. 1997. ESB Research Award 1996. Biophysical stimuli on cells during tissue differentiation at implant interfaces. *J. Biomech*. 30:539–548.
6. Mammoto, T., and D. E. Ingber. 2010. Mechanical control of tissue and organ development. *Development.* 137:1407–1420.
7. Riley, W. A., D. S. Freedman, …, G. S. Berenson. 1986. Decreased arterial elasticity associated with cardiovascular disease risk factors in the young. Bogalusa Heart Study. *Arteriosclerosis.* 6:378–386.
8. Huang, S., and D. E. Ingber. 2005. Cell tension, matrix mechanics, and cancer development. *Cancer Cell.* 8:175–176.
9. Kuznetsov, Y. G., A. J. Malkin, and A. McPherson. 1997. Atomic force microscopy studies of living cells: visualization of motility, division, aggregation, transformation, and apoptosis. *J. Struct. Biol*. 120:180–191.
10. Stamenović, D., B. Suki, …, J. J. Fredberg. 2004. Rheology of airway smooth muscle cells is associated with cytoskeletal contractile stress. *J. Appl. Physiol*. 96:1600–1605.
11. Brangwynne, C. P., F. C. MacKintosh, …, D. A. Weitz. 2006. Microtubules can bear enhanced compressive loads in living cells because of lateral reinforcement. *J. Cell Biol*. 173:733–741.
12. Fung, Y.-C. 1990. Biomechanics. Springer, New York.
13. Park, S., H. Hwang, …, W. S. Ryu. 2008. Enhanced *Caenorhabditis elegans* locomotion in a structured microfluidic environment. *PLoS ONE.* 3:e2550.
14. Sznitman, J., P. K. Purohit, …, P. E. Arratia. 2010. Material properties of *Caenorhabditis elegans* swimming at low Reynolds number. *Biophys. J*. 98:617–626.
15. Stephens, G. J., B. Johnson-Kerner, …, W. S. Ryu. 2008. Dimensionality and dynamics in the behavior of *C. elegans*. *PLOS Comput. Biol*. 4:e1000028.
16. Kindt, K. S., V. Viswanath, …, W. R. Schafer. 2007. *Caenorhabditis elegans* TRPA-1 functions in mechanosensation. *Nat. Neurosci*. 10:568–577.
17. O'Hagan, R., M. Chalfie, and M. B. Goodman. 2005. The MEC-4 DEG/ENaC channel of *Caenorhabditis elegans* touch receptor neurons transduces mechanical signals. *Nat. Neurosci*. 8:43–50.
18. Kiontke, K., and W. Sudhaus. 2006. Ecology of *Caenorhabditis* species (January 09, 2006), *WormBook*, ed. The *C. elegans* Research Community, WormBook, http://dx.doi.org/10.1895/wormbook.1.37.1, http://www.wormbook.org.
19. Park, S. J., M. B. Goodman, and B. L. Pruitt. 2007. Analysis of nematode mechanics by piezoresistive displacement clamp. *Proc. Natl. Acad. Sci. USA*. 104:17376–17381.
20. Nakajima, M., M. Ahmad, …, T. Fukuda. 2009. Local stiffness measurements of *C. elegans* by buckling nanoprobes inside an environmental SEM. *Proc. IEEE/RSJ Int. Conf. on Intelligent Robots and Systems*. IEEE, Piscataway, NJ. 4695–4700.
21. Harris, J., and H. Crofton. 1957. Structure and function in the nematodes: internal pressure and cuticular structure in *Ascaris*. *J. Exp. Biol*. 34:116–130.
22. Riddle, D. L., T. Blumenthal, …, J. R. Priess. 1997. *C. elegans* II, 3rd Ed. Cold Spring Harbor Laboratory Press, Cold Spring Harbor, NY.
23. Bird, A. F., and J. Bird. 1991. The Structure of Nematodes. Academic Press, New York.
24. Alexander, R. 1987. Bending of cylindrical animals with helical fibers in their skin or cuticle. *J. Theor. Biol*. 124:97–110.
25. Wainwright, S. A., F. Vosburgh, and J. H. Hebrank. 1978. Shark skin: function in locomotion. *Science.* 202:747–749.
26. Backholm, M., W. S. Ryu, and K. Dalnoki-Veress. 2013. Viscoelastic properties of the nematode *Caenorhabditis elegans*, a self-similar, shear-thinning worm. *Proc. Natl. Acad. Sci. USA*. 110:4528–4533.
27. Fung, Y.-C. 1970. Mathematical representation of the mechanical properties of the heart muscle. *J. Biomech*. 3:381–404.

28. Gardel, M. L., F. Nakamura, …, D. A. Weitz. 2006. Prestressed F-actin networks cross-linked by hinged filamins replicate mechanical properties of cells. *Proc. Natl. Acad. Sci. USA.* 103:1762–1767.
29. Lewis, J., and J. Fleming. 1995. Basic culture methods. *Methods Cell Biol.* 48:3–29.
30. Stiernagle, T. 2006. Maintenance of *C. elegans* (February 11, 2006), *WormBook*, ed. The *C. elegans* Research Community, WormBook, http://dx.doi.org/10.1895/wormbook.1.101.1, http://www.wormbook.org.
31. Hope, I. A. 1999. *C. elegans*: A Practical Approach. Oxford University Press, Oxford, UK.
32. Duerr, J. S. 2006. Immunohistochemistry (June 19, 2006), *WormBook*, ed. The *C. elegans* Research Community, WormBook, http://dx.doi.org/10.1895/wormbook.1.105.1, http://www.wormbook.org.
33. McDonald, J. C., and G. M. Whitesides. 2002. Poly(dimethylsiloxane) as a material for fabricating microfluidic devices. *Acc. Chem. Res.* 35:491–499.
34. Sia, S. K., and G. M. Whitesides. 2003. Microfluidic devices fabricated in poly(dimethylsiloxane) for biological studies. *Electrophoresis.* 24:3563–3576.
35. Abramoff, M. D., P. J. Magelhaes, and S. J. Ram. 2004. Image processing with IMAGEJ. *Biophotonics Int.* 11:36–42.
36. van Eede, M., D. Macrini, …, S. Dickinson. 2006. Canonical skeletons for shape matching. *Proc. 18th Int. Conf. on Pattern Recognition.* IEEE, Piscataway, NJ. 2:64–69.
37. Fang-Yen, C., L. Avery, and A. D. Samuel. 2009. Two size-selective mechanisms specifically trap bacteria-sized food particles in *Caenorhabditis elegans*. *Proc. Natl. Acad. Sci. USA.* 106:20093–20096.
38. Kégl, B., and A. Krzyzak. 2002. Piecewise linear skeletonization using principal curves. *IEEE Trans. Pattern Anal. Mach. Intell.* 24:59–74.
39. Lewis, D. L. 1997. A simple Boyle's law experiment. *J. Chem. Educ.* 74:209.
40. Moeendarbary, E., L. Valon, …, G. T. Charras. 2013. The cytoplasm of living cells behaves as a poroelastic material. *Nat. Mater.* 12:253–261.
41. Wang, H. 2000. Theory of Linear Poroelasticity with Applications to Geomechanics and Hydrogeology. Princeton University Press, Princeton, NJ.
42. Cox, G. N., M. Kusch, and R. S. Edgar. 1981. Cuticle of *Caenorhabditis elegans*: its isolation and partial characterization. *J. Cell Biol.* 90:7–17.
43. Brooks, A., G. J. Lithgow, and T. E. Johnson. 1994. Mortality rates in a genetically heterogeneous population of *Caenorhabditis elegans*. *Science.* 263:668–671.
44. Herndon, L. A., P. J. Schmeissner, …, M. Driscoll. 2002. Stochastic and genetic factors influence tissue-specific decline in aging *C. elegans*. *Nature.* 419:808–814.
45. Bailey, A. J., R. G. Paul, and L. Knott. 1998. Mechanisms of maturation and aging of collagen. *Mech. Ageing Dev.* 106:1–56.
46. von Mende, N., D. M. Bird, …, D. L. Riddle. 1988. *dpy-13*: a nematode collagen gene that affects body shape. *Cell.* 55:567–576.
47. Page, A. P., and I. L. Johnstone. 2007. The cuticle (March 19, 2007), *WormBook*, ed. The *C. elegans* Research Community, WormBook, http://dx.doi.org/10.1895/wormbook.1.138.1, http://www.wormbook.org.
48. Russ, J. C. 2010. The Image Processing Handbook. CRC Press, Boca Raton, FL.
49. Landau, L. D., and E. Lifshitz. 1986. Theory of Elasticity, Vol. 7. Course of Theoretical Physics, 3rd Ed. Butterworth-Heinemann, Oxford, UK.
50. Sun, A. Y., and E. J. Lambie. 1997. gon-2, a gene required for gonadogenesis in *Caenorhabditis elegans*. *Genetics.* 147:1077–1089.
51. Storm, C., J. J. Pastore, …, P. A. Janmey. 2005. Nonlinear elasticity in biological gels. *Nature.* 435:191–194.
52. Goodman, M. B. 2006. Mechanosensation (January 06, 2006), *WormBook*, ed. The *C. elegans* Research Community, WormBook, http://dx.doi.org/10.1895/wormbook.1.62.1, http://www.wormbook.org.
53. Fang-Yen, C., M. Wyart, …, A. D. Samuel. 2010. Biomechanical analysis of gait adaptation in the nematode *Caenorhabditis elegans*. *Proc. Natl. Acad. Sci. USA.* 107:20323–20328.
54. Wainwright, S. A. 1982. Mechanical Design in Organisms. Princeton University Press, Princeton, NJ.
55. Liu, A. J., and S. R. Nagel. 2010. The jamming transition and the marginally jammed solid. *Annu. Rev. Condens. Matter Phys.* 1:347–369.
56. Trappe, V., V. Prasad, …, D. A. Weitz. 2001. Jamming phase diagram for attractive particles. *Nature.* 411:772–775.
57. Baranau, V., and U. Tallarek. 2014. On the jamming phase diagram for frictionless hard-sphere packings. *Soft Matter.* 10:7838–7848.

Worms under pressure: bulk mechanical properties of *C. elegans* are independent of the cuticle

William Gilpin[1], Sravanti Uppaluri[2], Clifford P. Brangwynne[2*]

[1]Department of Physics, [2]Department of Chemical and Biological Engineering,
Princeton University, Princeton, NJ 08544 USA

[*]To whom correspondence should be addressed; E-mail: cbrangwy@princeton.edu

Supplementary Information

Analysis of poroelastic effects

If water efflux played a role, the worm would appear stiffer over short timescales due to trapped, incompressible fluid increasing the observed, "poroelastic" modulus. Previous estimates of the poroelasticity of living systems have estimated a characteristic timescale of ∼10 s for poroelastic effects in single cells (1). Applying a similar reasoning to the worm, the characteristic timescale for poroelastic relaxation should be $\tau_p \propto L^2/D_p$, where D_p is a reduced diffusivity of water in the worm that takes into account the effects of porosity. The characteristic length L that water needs to diffuse in order to exit the worm is on the order of the diameter of the worm, L ∼100 μm. The poroelastic diffusivity depends inversely on the characteristic pore size, $D_p = E\xi^2/\eta$, where E is the observed modulus for the worm's body in the absence of embedded fluid, ξ is the pore size, and η is the viscosity of water, $\eta \sim .001Pa\ s$. Even using a small characteristic pore size of 100 nm, roughly 10 times smaller than the spacing between annuli on the cuticle (2), results in a characteristic poroelastic diffusion timescale $\tau_d = 1 \times 10^{-2}\ s$; this is four orders of magnitude smaller than our experimental timescales (100 s). In the poroelasticity literature, mechanics measurements in this regime are referred to as the "drained modulus", in which water efflux from the system is not limiting (3).

Description of image correlation analysis

The Digital Image Correlation image processing routine, often referred to as Particle Imaging Velocimetry, generates a vector field representing the displacement of a coordinate system on an object's body relative to a coordinate system fixed to the rectangular image frame. In the first frame of a time series, the body coordinates are defined as a subset of a fixed coordinate system defined over the entire frame. In successive frames, the body in the image undergoes deformations that change the locations of the body coordinates relative to the initial coordinates. For the analysis of strain in an elastic body, displacement fields are generated using pairs of consecutive images only: the fixed coordinates are re-initialized for each image, and displacements are then calculated using just the displacement of the body coordinates in the next image relative to the current image. To implement cross correlation efficiently for each successive pair in a large time series, an analogue of the convolution theorem was exploited that allowed the cross-correlation to be computed rapidly using the discrete Fourier transforms (4). For the image types used in the experiment, the essential assumptions necessary for the use of the Fourier transform were met for the frequency ranges

of interest.

Post-Processing and Evaluation of Strain

The vector field $\mathbf{u} = (u(i,j), v(i,j))$ generated by the cross-correlation analysis contains many artifacts due to poor correlations and undersampling, and so the vector field is post-processed using outlier rejection, spatial averaging, and temporal averaging. The range of images or spatial width of the filters vary depending on the magnification and lighting conditions, as well as the timescales of the deformations being observed. Once the smoothed displacement vector field $\mathbf{u}$ is generated, it will generally contain vectors with physically unattainable displacements, usually due to the algorithm misidentifying a correlation between two similar objects in subsequent images as being the displacement of a single object. Because of the strong dependence of these outliers on the specific composition and contents of the images, these outliers are manually rejected by defining appropriate truncation limits in a histogram showing the magnitudes of all vectors in $\mathbf{u}$.

Direct measurement of pressure using a mechanical gauge

In order to directly measure the pressure within the device and confirm its proximity to values predicted by Boyles Law, the syringe and syringe pump were connected directly to a liquid-filled, bourdon tube pressure gauge (065°C, 1% accuracy; McMaster-Carr, Atlanta, GA). The syringe was then depressed using the syringe pump using the standard 15 minute pressurization sequence used in many of the experiments, and the resulting plot is shown in Figure S1.

For the experiments, the gauge and general setup were degassed in a vacuum chamber and then allowed to settle in order to remove dissolved or trapped air that could affect the accuracy of the measurement. It was observed that the final pressure recorded in the device differed from that predicted by Boyles law, but that this difference decreased with longer degassing times, suggesting that this discrepancy is negligible in the actual experiments, in which trapped air pockets would be readily observable in the transparent, sealed microfluidic chamber.

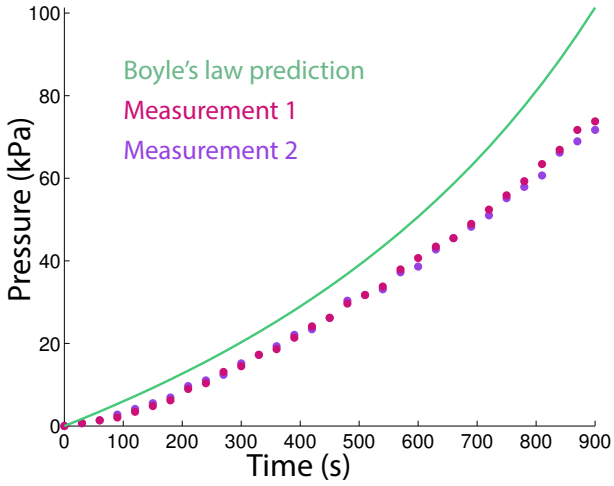

Figure S1 The pressure in the syringe versus time as the volume in the syringe is gradually decreased over 15 minutes. The solid line indicates the prediction of Boyle's law.

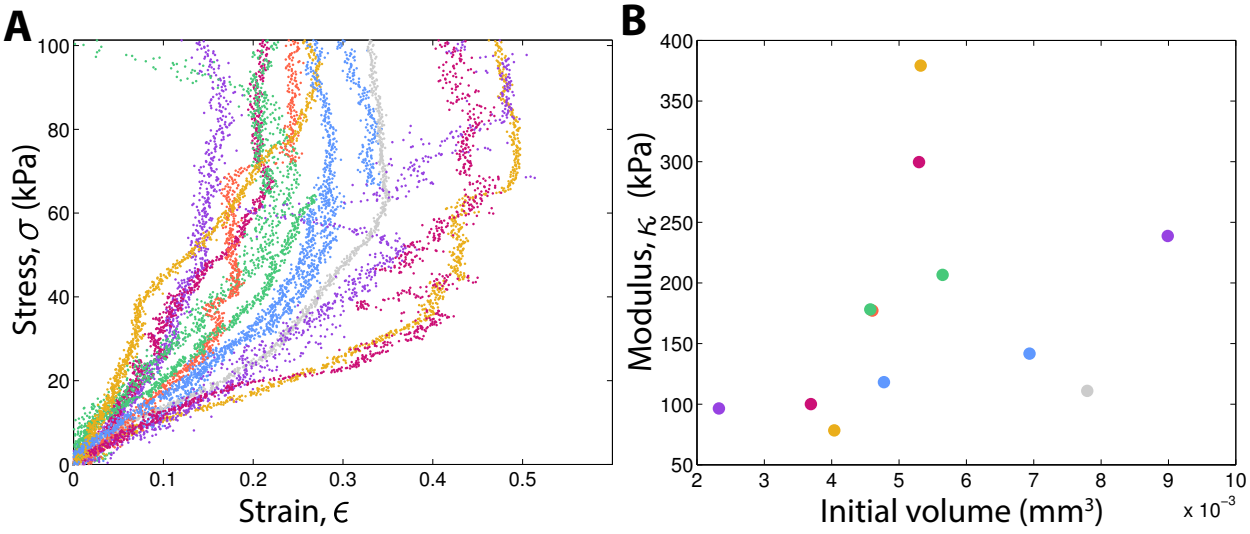

Figure S2 *(A)* Stress-strain curves for dead young adult worms *(B)* The bulk modulus versus initial volume.

Supporting References

1. Moeendarbary, E., L. Valon, M. Fritzsche, A. R. Harris, D. A. Moulding, A. J. Thrasher, E. Stride, L. Mahadevan, and G. T. Charras, 2013. The cytoplasm of living cells behaves as a poroelastic material. *Nature materials* 12:253–261.

2. Riddle, D. L., T. Blumenthal, B. J. Meyer, J. R. Priess, et al., 1997. *C. elegans* II. Cold Spring Harbor Laboratory Press, 3 edition.

3. Wang, H., 2000. Theory of linear poroelasticity with applications to geomechanics and hydrogeology. Princeton University Press.

4. Russ, J. C., 2010. The image processing handbook. CRC press.